Smoothing and coherent structure formation in organic-organic heterostructure growth

A. Hinderhofer[1(a)], A. Gerlach[1], S. Kowarik[1,2], F. Zontone[3], J. Krug[4] and F. Schreiber[1]

[1] *Institut für Angewandte Physik Universität Tübingen - 72076 Tübingen, Germany, EU*
[2] *Department of Chemistry, University of California - Berkeley, CA 94720, USA*
[3] *ESRF - 6 Rue Jules Horowitz, BP 220, 38043 Grenoble Cedex 9, France, EU*
[4] *Institut für Theoretische Physik, Universität zu Köln - 50937 Köln, Germany, EU*

Abstract – We use *in situ* real-time X-ray reflectivity and complementary atomic force microscopy to monitor crystallinity and roughness evolution during growth of organic heterostructures, *i.e.* perfluoropentacene (PFP) on diindenoperylene (DIP) and pentacene (PEN) on PFP. For both systems, surface smoothing during thermal evaporation of the second material on top of the first is observed. The smoothing can be rationalized by a, compared to homoepitaxy, lowered step edge barrier for one species diffusing on the other. In addition, we find an exceptionally well-ordered interface for PEN-on-PFP growth and PEN growth with anomalously low roughening, along with coherent scattering over the entire thickness.

Introduction. – The surface morphology and roughness of thin films and crystals depend on competing mechanisms, which either roughen or smooth the film surface during growth. Important roughening mechanisms, which tend to be dominating in most cases, are kinetic roughening based on shot noise and roughening due to mound growth, which is facilitated by reduced interlayer transport, often associated with a step edge, or Ehrlich-Schwoebel barrier. While these issues have been relatively well studied for growth of simple atomic species [1–3], comparatively little is known about organic systems. These are expected to exhibit a fundamentally different growth behavior, due to their different dominating interactions (van der Waals) and thus different response to strain and also due to their internal degrees of freedom (tilt angle as well as vibrational excitations and thus additional thermalisation channels).

In crystalline organic thin-film growth, usually high diffusion lengths in the range of several micrometers [4] are possible, but also high step edge barriers of $\approx 0.7\,\mathrm{eV}$ have been reported [5,6]. Recently several interesting and new features for organic growth have been reported including anomalous rapid roughening [7–9], deep grain boundaries [10] and thickness-dependent step edge

barriers [5,11,12]. Theoretical models show that by neglecting the step edge barrier roughening would be strongly reduced [13]. These findings suggest that mound growth, induced by high step edge barriers, often dominates the roughness evolution for crystalline organic thin films.

The situation is more complex for growth of organic-organic heterostructures [14], which are important for many device applications like organic photovoltaic cells or organic light-emitting diodes. In this letter we present the roughness evolution for organic-organic heterostructures and evidence for smoothing. We also show that if the out-of-plane crystal lattice spacing of both materials is sufficiently similar, the smoothing effect can be accompanied by a structure that scatters X-rays coherently even from the organic-organic interface.

Experimental. – Thin films of diindenoperylene (DIP; $C_{32}H_{16}$; fig. 1(a)), perfluoropentacene (PFP; $C_{22}F_{14}$; fig. 1(a)) and pentacene (PEN; $C_{22}H_{14}$) were evaporated on silicon wafers with a 1.5 nm thick native oxide layer in ultra-high vacuum (base pressure $< 5 \cdot 10^{-9}\,\mathrm{mbar}$) by thermal evaporation. The substrate temperature T was held at $30\,^{\circ}\mathrm{C}$. The growth rate for all molecules was between 0.1 and $0.2\,\mathrm{nm/min}$ and monitored via X-ray reflectivity. *In situ* X-ray reflectivity

(a)E-mail: alexander.hinderhofer@uni-tuebingen.de

Fig. 2: (Colour on-line) Real-time X-ray data from growth of a PFP-on-DIP heterostructure. The white arrow denotes the onset of PFP evaporation on top of the DIP layer. The dark arrows point to the time slice after 3 nm of PFP evaporation.
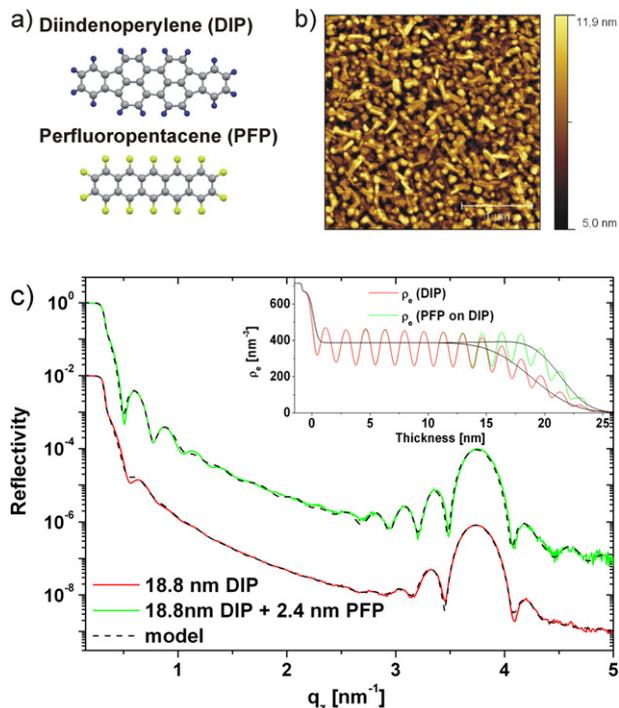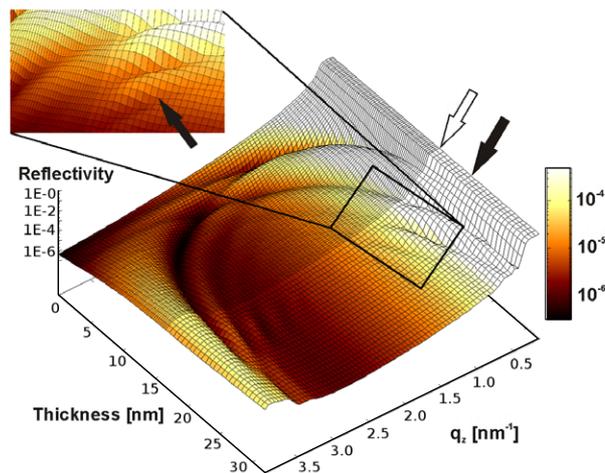
Fig. 1: (Colour on-line) (a) DIP ($C_{32}H_{16}$) and PFP ($C_{22}F_{14}$). (b) AFM image from PFP-on-DIP ($3 \times 3 \mu m$). (c) X-ray reflectivity data from a PFP-on-DIP heterostructure ($d_{PFP} = 2.4$ nm and $d_{DIP} = 18.4$ nm) and from the underlying DIP layer. For clarity the DIP curve was shifted by two orders of magnitude. The inset shows electron density profiles ρ_e of the two films, the black lines denote the average for extracting roughness and thickness parameters.

measurements were performed either with a GE XRD 3003TT diffractometer using $Cu\,K_{\alpha 1}$ radiation ($\lambda = 0.151$ nm) or at beamline ID10B ($\lambda = 0.092$ nm) of the ESRF in Grenoble, France. Modeling and fitting of X-ray reflectivity data were done with MOTOFIT using the Parratt formalism [15].

Tapping mode AFM-data were analyzed with the Gwyddion software. The power spectral density function (PSDF) is extracted from AFM images and gives the distribution of spatial frequencies of the surface. For extracting the PSDF from AFM images only line scans in the fast scan axis were analyzed. For each PSDF we averaged the data from two AFM images from different spots to reduce noise. In the literature several methods have been described for extracting the lateral correlation length ξ from AFM images [9,16]. We determined ξ by converting the characteristic bend in the PSDF directly to a real space length [16]. Since absolute values for ξ can vary strongly with the method used the error bars for the absolute values are large. However, for this publication more relevant are relative changes in ξ between different stages of growth for which the error is below 5%.

PFP on DIP. – Before discussing the time evolution of the surface roughness, we consider post-growth

X-ray data of a PFP-on-DIP heterostructure (2.4 nm PFP corresponding to 1.5 monolayers on 18.8 nm DIP) and compare it with data from the underlying DIP layer (fig. 1(c)). The out-of-plane lattice spacings of DIP and PFP determined to be 1.65 nm and 1.57 nm (electron density profile ρ_e, inset fig. 1(c)), respectively correspond to their thin-film phases [14,17–19]. This assignment was confirmed by grazing incidence X-ray diffraction (GIXD). Strain-induced deviation of the GIXD features of PFP and DIP in the heterostructure from the single-layer phase was determined to be less than 0.5%. An important result of fig. 1(c) is that the root mean squared roughness σ of the PFP-on-DIP heterostructure ($\sigma_{PFP} = 2.0 \pm 0.1$ nm) as determined from the Kiessig oscillations is significantly lower than that of the underlying DIP film ($\sigma_{DIP} = 2.9 \pm 0.1$ nm).

The resulting surface morphology of the PFP-on-DIP heterostructure was characterized by atomic force microscopy (AFM, fig. 1(b)). By AFM the roughness was determined to be $\sigma_{PFP} = 1.9 \pm 0.2$ nm which agrees well with σ_{PFP} obtained from X-ray reflectivity and confirms the smoothing of the heterostructure. The surface of the film exhibits round grains of DIP and needle-like grains of PFP. Obviously, complete wetting of the DIP film does not occur and the diffusion length of PFP has to be high, since after evaporation of 1.5 monolayers of PFP large PFP crystals are observed. In addition, the PFP grains have their centers mostly in the gaps between the DIP grains.

To follow the roughness evolution of a PFP-on-DIP heterostructure in more detail, X-ray reflectivity was measured in real-time during growth (fig. 2) [7]. After depositing 16 nm DIP (denoted by the white arrow), PFP was grown on top of this layer. Shortly after starting PFP evaporation pronounced Kiessig oscillations are observed (dark arrows), which are damped out again for higher
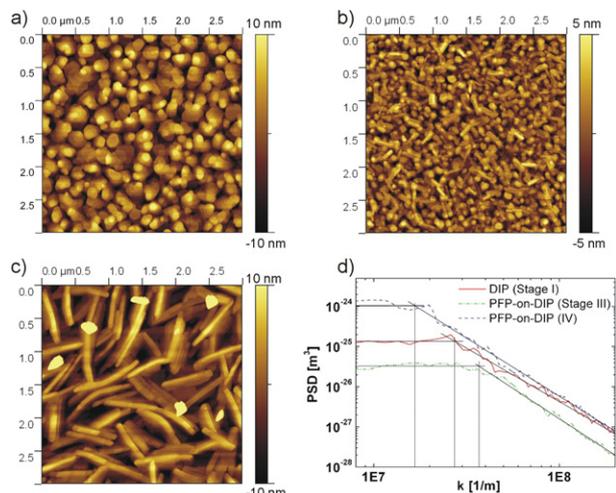
Fig. 3: (Colour on-line) AFM images at different growth stages from PFP-on-DIP growth: (a) stage I, (b) stage III, (c) stage IV; (d) power spectral density function extracted from the corresponding AFM images. Black lines are guides to the eye.
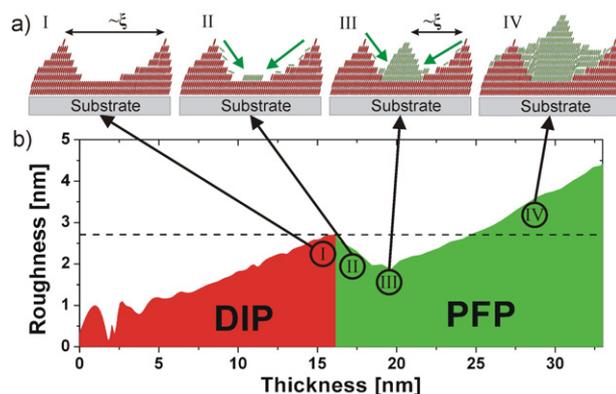

Fig. 4: (Colour on-line) a) Growth scenario of PFP islands on DIP. b) Roughness evolution of a PFP-on-DIP heterostructure, extracted from the reflectivity data in fig. 2.

PFP-thicknesses. From these features the roughness for each thickness can be extracted (see fig. 4(b)). While the roughness σ of the pristine DIP film is 2.7 ± 0.1 nm, after deposition of 3.2 nm PFP the heterostructure shows a minimal surface roughness of only 1.9 ± 0.1 nm. A prerequisite for this roughness reduction is a low step edge barrier, that allows interlayer diffusion of the molecules and facilitates an efficient molecular downhill-current.

For growth of atomic systems on rough substrates (*e.g.* InAs buffer layers) it was found using continuum growth theory and kinetic Monte Carlo simulations that under certain conditions the competing mechanisms of smoothing and roughening can lead to a minimum in the roughness evolution even though both materials exhibit step edge-barrier–dominated growth [20–22]. In this case, a minimum can occur because of the dependence of the roughening and smoothing rates on the spatial frequency f of the surface modulation. Specifically, during mound formation low-frequency modes within an interval $0 < f < f_c$ grow in amplitude while those with $f > f_c$ are damped by surface diffusion [3]; here f_c is a characteristic frequency related to the length scale of the incipient mounds. Since the surface roughness is given by an integral over the PSDF of the surface, in the early stages of overlayer growth, the smoothing at high f can overcompensate the roughening at low f such that σ transiently decreases.

By analyzing the PSDF extracted from AFM images at different growth stages (fig. 3) we find for our system around the roughness minimum (fig. 4(a), III) smoothing at all frequencies, but in particular at *low* f. This qualitatively new observation is in contrast to reports for InAs growth that low spatial frequencies are unstable from the beginning. After this initial smoothing, roughening at all frequencies sets in (fig. 4(a), IV). We conclude that the mechanism proposed in refs. [20–22], which relies on

frequency-dependent smoothing and roughening rates, is not applicable in our system.

A simplified heterostructure growth scenario consistent with the findings above is summarized in fig. 4(a), I–IV. Stage I shows the rough DIP surface directly before PFP evaporation. The lateral correlation length associated with the grain-grain distance of such a DIP film is $\xi \approx 230$ nm, as extracted from AFM data. At stage II PFP molecules hit the DIP surface and start diffusing. To enable a downhill current the step edge barrier has to be overcome by the thermal energy of the PFP molecules, *i.e.* the step edge barriers have to be lower for PFP molecules diffusing on a crystalline DIP surface compared to PFP diffusing on a PFP surface. The PFP molecules then accumulate and crystallize in the gaps of the DIP film. The intermediate growth stage III depicts the minimum of the roughness evolution. There PFP grains between the DIP grains have formed and filled up the space between the DIP grains (fig. 1(b)). At this stage the surface exhibits grains of two different species, and the lateral correlation length is reduced to $\xi \approx 170$ nm. This filling of gaps between DIP grains works on long length scales and therefore leads to the decreasing contribution of low spatial frequencies to the total roughness. During later growth stages (fig. 4(a), IV) the heterostructure roughens fast and PFP forms large needles ($\xi \approx 370$ nm), which is also typical for PFP growth on substrates like SiO_2 [17]. Note, that an increase of the lateral length scale from the first to the second layer, which forms the heterostructure, is a prerequisite for observing a nonmonotonic roughness evolution also within the theoretical framework of [21,22].

PEN on PFP. – Probably still more interesting than DIP/PFP is the combination of two materials with a maximum structural compatibility, but different electronic properties, namely PEN/PFP, since it offers the possibility for growth of an interface that is still better ordered. Indeed, the structural compatibility of PEN/PFP was recently demonstrated by coevaporation of both molecules into one molecular mixed crystal [14].
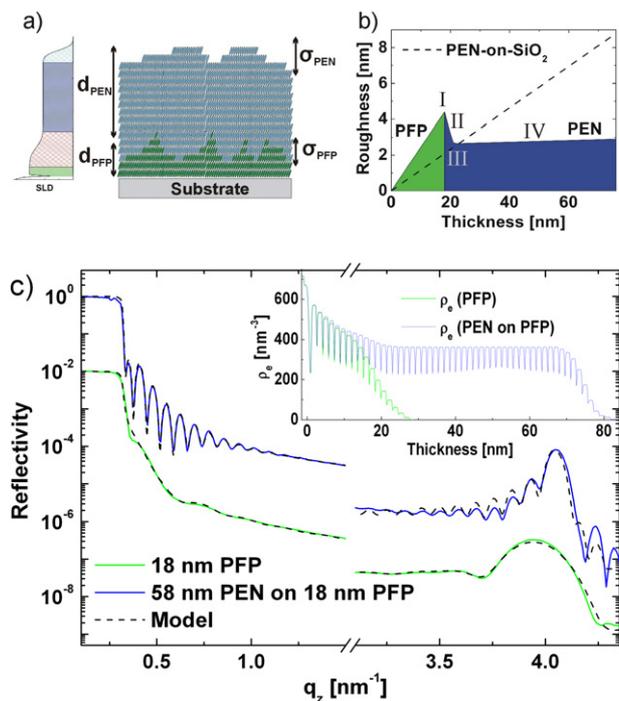
Fig. 5: (Colour on-line) (a) Heterostructure with thicknesses of the organic layers d_{PFP} and d_{PEN} and roughness of the intermediate interface σ_{PFP} and the top-roughness σ_{PEN}. (b) Roughness evolution during film growth. (c) Reflectivity data and fits from a 18 nm thick PFP film, and from a PEN-on-PFP heterostructure with $d_{PFP} = 18$ nm and $d_{PEN} = 58$ nm. The inset shows ρ_e for both fits.

Figure 5(a) shows a schematic and the electron density profile ρ_e of the analyzed heterostructure, fig. 5(c) two X-ray reflectivity scans of the underlying PFP film with a thickness of $d_{PFP} = 18$ nm and the PEN-on-PFP heterostructure with $d_{PFP} = 18$ nm and $d_{PEN} = 58$ nm. The inset shows the modeled ρ_e for both datasets, from which the PFP (PEN) out-of-plane lattice spacing was found to be 1.57 nm (1.55 nm). The PFP out-of-plane lattice spacing correspond to the thin-film structure determined on native SiO_2 [18], for PEN, however, the out-of-plane lattice spacing is slightly larger than on native SiO_2 (1.54 nm) [23]. A fit of the Kiessig oscillations (fig. 5(c)) yields $\sigma_{PFP} = 4.4 \pm 0.1$ nm and $\sigma_{PEN} = 2.9 \pm 0.1$ nm, respectively, *i.e.* we again find a smoothing effect. Real-time X-ray reflectivity of the side fringes of the first Bragg reflection around $q_z = 0.41 \, \text{Å}^{-1}$, so-called Laue oscillations, indicates the roughness evolution (fig. 5(b)). The lowest roughness is reached at ≈ 3 nm of PEN evaporation ($\sigma_{PEN} = 2.7 \pm 0.2$ nm).

Compared to PFP-on-DIP, PEN-on-PFP behaves in a similar way for growth stages sketched in fig. 4(a), I–III. This observation of smoothing of an organic-organic heterostructure for a second material combination suggests that this phenomenon is not specific to one system, but can be observed for a broader range of materials. Note, however, that, *e.g.*, the reverse order of deposition (PFP-on-PEN and DIP-on-PFP), does not
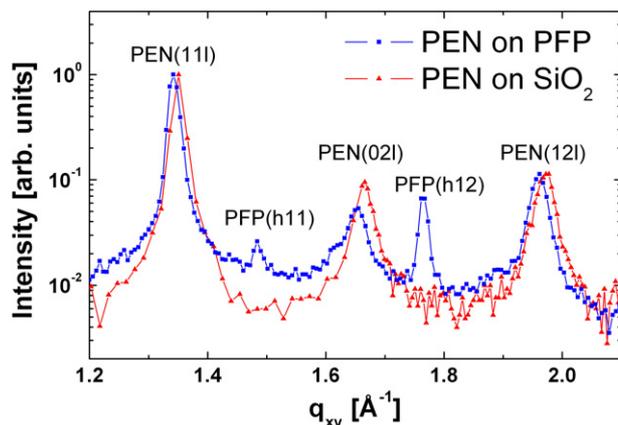

Fig. 6: (Colour on-line) GIXD data from PEN on SiO_2 (20 nm) and PEN (20 nm) grown on PFP (15 nm).

lead to smoothing. This is not surprising when considering the different interactions between, for example, a diffusing DIP molecule with a PFP crystal *vs.* a PFP molecule with a DIP crystal. Importantly, after completion of the smoothing regime in stage III, the two material systems behave qualitatively different in stage IV. For PFP-on-DIP, PFP exhibits typical fast roughening (fig. 4(b)). In contrast, for PEN-on-PFP growth the PEN roughness increases only very slowly after the smoothing is completed (fig. 5(b)). Compared to PEN growth on SiO_2, where the roughening at this growth temperature is fast (broken line in fig. 5(b)) [23], the roughening of PEN is nearly completely suppressed for growth on a PFP film. For crystalline organic thin-film growth usually fast roughening sets in after few layers of growth [7–9]. Therefore, slow or suppressed roughening of PEN is very unusual, particularly considering the high crystallinity of the film.

In this context an important observation is that the qualitative difference in roughening behavior for the PEN-on-PFP system compared to the PFP-on-DIP structure or PEN on SiO_2 is accompanied by the formation of an exceptionally well-ordered interface. The spacing of the Laue oscillations around the first Bragg reflection at $q_z = 0.41 \, \text{Å}^{-1}$ of the heterostructure agrees with that of the Kiessig oscillations, implying that the PEN-on-PFP film scatters X-rays coherently over the entire thickness without significant phase change at the interface. This interface formation is possible because the out-of-plane lattice spacings of PEN (1.55 nm) and PFP (1.57 nm) are relatively similar. From the coherent scattering over the entire heterostructure we conclude that no disordered molecular layer (for example lying molecules) is formed at the interface. Instead, the partly filled layers at the PFP surface are successively filled by standing PEN molecules.

Since the PEN out-of-plane lattice spacing is slightly larger than for growth on SiO_2, slightly smaller lateral unit cell parameters can be expected. Indeed, the GIXD peak positions from PEN-on-PFP deviate up to 1% from GIXD data of PEN on SiO_2 (fig. 6). In organic thin-film

growth even small changes of the unit cell dimensions and in particular the molecular tilt angle can have a large impact on the step edge barrier and therefore on the roughening behavior [5,11]. Since the structural order at the interface is very high, the PFP film appears to serve as a template for a slightly relaxed thin-film PEN structure. One might speculate that this facilitates the observed higher interlayer transport compared to PEN growth on SiO_2.

Summary. – In summary, we demonstrated surface smoothing for organic heterostructures. A low step edge barrier for certain molecules (PFP, PEN) diffusing on a molecular crystalline surface of a different species (DIP, PFP) can explain the smoothing effect. In this case crystals of the second material nucleate preferably in the gaps of the first material, where molecules accumulate and form crystalline grains. This leads to a filling of voids and to a reduced roughness of the heterostructure surface. In particular, smoothing develops at low spatial frequencies, *i.e.* long wavelengths which is in contrast to growth models of atomic systems. Within our parameter range ($d = 10, \ldots, 20$ nm; $T = 10, \ldots, 50\,^{\circ}$C) the presented smoothing effect is qualitatively reproducible for different thicknesses d and growth temperatures. In addition, we find an exceptionally well-ordered interface for PEN-on-PFP heterostructures, which yields a relaxed PEN structure, for which roughening, compared to growth on SiO_2, is strongly suppressed. This observation demonstrates that roughening for organic thin-film growth can be influenced effectively by templating layers that leave the crystalline structure nearly unchanged. Material combinations such as those presented here may be used as model cases for organic-organic interface engineering.

$$* * *$$

REFERENCES

[1] Krug J., *Adv. Phys.*, **46** (1997) 139.
[2] Pimpinelli A. and Villain J., *Physics of Crystal Growth* (Cambridge University Press) 1988.
[3] Michely T. and Krug J., *Islands, Mounds and Atoms* (Springer, Berlin Heidelberg) 2004.
[4] Meyer zu Heringdorf F. J., Reuter M. C. and Tromp R. M., *Nature*, **412** (2001) 517.
[5] Hlawacek G., Puschnig P., Frank P., Winkler A., Ambrosch-Draxl C. and Teichert C., *Science*, **321** (2008) 108.
[6] Fendrich M. and Krug J., *Phys. Rev. B*, **76** (2007) 121302.
[7] Kowarik S., Gerlach A., Sellner S., Schreiber F., Cavalcanti L. and Konovalov O., *Phys. Rev. Lett.*, **96** (2006) 125504.
[8] Dürr A. C., Schreiber F., Ritley K. A., Kruppa V., Krug J., Dosch H. and Struth B., *Phys. Rev. Lett.*, **90** (2003) 016104.
[9] Yim S. and Jones T. S., *Phys. Rev. B.*, **73** (2006) 161305.
[10] Yim S. and Jones T. S., *Appl. Phys. Lett.*, **94** (2009) 021911.
[11] Zhang X., Barrena E., Goswami D., de-Oteyza D. G., Weis C. and Dosch H., *Phys. Rev. Lett.*, **103** (2009) 136101.
[12] Krause B., Schreiber F., Dosch H., Pimpinelli A. and Seeck O. H., *Europhys. Lett.*, **65** (2004) 372.
[13] Zorba S., Shapir Y. and Gao Y., *Phys. Rev. B*, **74** (2006) 245410.
[14] Salzmann I., Duhm S., Heimel G., Rabe J. P., Koch N., Oehzelt M., Sakamoto Y. and Suzuki T., *Langmuir*, **24** (2008) 7294.
[15] Andrew N., *J. Appl. Cryst.*, **39** (2006) 273.
[16] Constantoudis V., Patsis G. P., Tserepi A. and Gogolides E., *J. Vac. Sci. Technol. B*, **21** (2003) 1019.
[17] Hinderhofer A., Heinemeyer U., Gerlach A., Kowarik S., Jacobs R. M. J., Sakamoto Y., Suzuki T. and Schreiber F., *J. Chem. Phys.*, **127** (2007) 194705.
[18] Kowarik S., Gerlach A., Hinderhofer A., Milita S., Borgatti F., Zontone F., Suzuki T., Biscarini F. and Schreiber F., *Phys. Status Solidi (RRL)*, **2** (2008) 120.
[19] Dürr A. C., Schreiber F., Münch M., Karl N., Krause B., Kruppa V. and Dosch H., *Appl. Phys. Lett.*, **81** (2002) 2276.
[20] Gyure M., Zinck J. J., Ratsch C. and Vvedensky D. D., *Phys. Rev. Lett.*, **81** (1998) 4931.
[21] Krug J. and Rost M., *Phys. Rev. B*, **60** (1999) R16334.
[22] Castellano C. and Krug J., *Phys. Rev. B*, **62** (2000) 2879.
[23] Ruiz R., Choudhary D., Nickel B, Chang T. T. K., Mayer A., Clancy P., Blakely J. M., Headrick R. L., Iannotta S. and Malliaras G. G., *Chem. Mater.*, **16** (2004) 4497.